Journal of Nuclear Materials 462 (2015) 43–53

Contents lists available at ScienceDirect

Journal of Nuclear Materials

journal homepage: www.elsevier.com/locate/jnucmat

Thermodynamic assessment of the LiF–ThF_4–PuF_3–UF_4 system

E. Capelli [a,b], O. Beneš [a,*], R.J.M. Konings [a,b]

[a] European Commission, Joint Research Centre, Institute for Transuranium Elements, P.O. Box 2340, 76125 Karlsruhe, Germany
[b] Department of Radiation Science and Technology, Faculty of Applied Physics, Delft University of Technology, Delft 2629JB, The Netherlands

ARTICLE INFO

Article history:
Received 17 October 2014
Accepted 20 March 2015
Available online 26 March 2015

ABSTRACT

The LiF–ThF_4–PuF_3–UF_4 system is the reference salt mixture considered for the Molten Salt Fast Reactor (MSFR) concept started with PuF_3. In order to obtain the complete thermodynamic description of this quaternary system, two binary systems (ThF_4–PuF_3 and UF_4–PuF_3) and two ternary systems (LiF–ThF_4–PuF_3 and LiF–UF_4–PuF_3) have been assessed for the first time. The similarities between CeF_3/PuF_3 and ThF_4/UF_4 compounds have been taken into account for the presented optimization as well as in the experimental measurements performed, which have confirmed the temperatures predicted by the model. Moreover, the experimental results and the thermodynamic database developed have been used to identify potential compositions for the MSFR fuel and to evaluate the influence of partial substitution of ThF_4 by UF_4 in the salt.

1. Introduction

Mixtures of fluoride salts, such as the studied LiF–ThF_4–PuF_3–UF_4 system, are currently considered as fuel for the Molten Salt Fast Reactor (MSFR) [1]. This reactor design, which is a liquid fuelled fast (epi-thermal) spectrum reactor, can be well adapted to the thorium fuel cycle ($^{232}Th/^{233}U$) which offers several advantages and meets the Generation IV goals. Since ^{232}Th is not fissile, an initial load of fissile material has to be added to the fuel for the reactor start-up and the possibility of starting molten salt reactors with plutonium trifluoride PuF_3 has been demonstrated in early studies at Oak Ridge National Laboratories [2,3] and more recently by Merle-Lucotte et al. [4]. The advantage of this design is the possibility to burn plutonium and minor actinides produced in the LWRs (Light Water Reactor) and produce ^{233}U needed to supply the fissile material for the $^{232}Th/^{233}U$ cycle. In the proposed salt composition, the LiF salt is used as solvent for both fertile (ThF_4) and fissile (PuF_3) material with relative concentrations given by neutronic and physico-chemical requirements. Moreover, UF_4 must be added to control the redox potential of the fuel via the UF_4/UF_3 ratio.

In this work, we present the thermodynamic assessment of the LiF–ThF_4–PuF_3–UF_4 system. The binary and ternary phase diagrams containing PuF_3 have been assessed for the first time based on the similarities of the proxy compounds (CeF_3/PuF_3 and ThF_4/UF_4, respectively) and on the experimental data available in the literature. All thermodynamic assessments were done according to the Calphad method using the two sublattice model for the description of the solid solutions and the modified quasi-chemical model for the description of the liquid solution. In order to validate the model developed, some selected LiF–CeF_3–ThF_4 ternary compositions have been synthesized and analysed using the Differential Scanning Calorimeter (DSC). The obtained equilibrium data have been used to optimize ternary parameters in the model so that a good agreement with the experiment has been achieved. As last step, the thermodynamic database developed and the experimental results have been used to optimize the MSFR fuel composition. Based on different criteria, several potential compositions have been identified and the influence of ThF_4 substitution with UF_4 have been investigated. In fact, this action may be useful for proliferation issues as well as for neutronic considerations.

2. Thermodynamic modeling

In this work, we performed the thermodynamic assessment of the LiF–ThF_4–PuF_3–UF_4 quaternary system. The binary systems ThF_4–PuF_3 and UF_4–PuF_3 and the ternary systems LiF–ThF_4–PuF_3 and LiF–UF_4–PuF_3 have been assessed for the first time while the remaining sub-systems have been taken from previous works [5,6]. During the optimization, due to the lack of experimental data, the two following assumptions have been taken into account:

1. CeF_3 is considered as proxy compound to PuF_3.
2. ThF_4 is considered as proxy compound to UF_4.

Both assumptions are based on strong similarity of the properties of the paired compounds as experimentally evidenced for both

* Corresponding author. Tel.: +49 7247 951 385; fax: +49 7247 951 99385.
E-mail address: ondrej.benes@ec.europa.eu (O. Beneš).

http://dx.doi.org/10.1016/j.jnucmat.2015.03.042
0022-3115/

cases and discussed in more details in our previous work [6]. It must be mentioned here that the analogy between UF_4 and ThF_4 compounds is valid only to a certain extent. In fact, there are some differences in the chemical behaviour of the two compounds, such as the possible oxidation state of uranium in the fluoride media compared to thorium which can only be tetravalent and the stoichiometry of the intermediate compounds formed in the binary systems LiF–ThF_4 and LiF–UF_4. However, the general shape of the liquidus lines for the LiF–ThF_4 and LiF–UF_4 systems are similar and the liquidus temperatures are almost identical for UF_4 content less than 23 mol%. This is particularly important for our application where the liquidus lines are of primary importance and the UF_4 content is kept small. As consequence of the assumptions made, the binary systems ThF_4–PuF_3 and UF_4–PuF_3 and the ternary systems LiF–ThF_4–PuF_3 and LiF–UF_4–PuF_3 have been assessed using the same excess Gibbs parameters as obtained for the Th- and Ce-containing systems presented in our previous paper [6].

All thermodynamic assessments performed in this study have been done according to the Calphad method using the FactSage software [7], as described throughout the next sections.

2.1. Compounds

The first step for a thermodynamic assessment is the definition of the Gibbs energy of pure compounds, which is given by the following relation:

$$G(T) = \Delta_f H^0(298) - S^0(298)T + \int_{298}^{T} C_p(T)dT - T \times \int_{298}^{T} \left(\frac{C_p(T)}{T}\right)dT, \quad (1)$$

where $\Delta_f H^0(298)$ and $S^0(298)$ are respectively the standard enthalpy of formation and standard absolute entropy, both referring to a temperature of 298.15 K and $C_p(T)$ is the temperature function of the heat capacity at constant pressure. The thermodynamic data for all compounds used in this work are reported in Table 1. The data of four intermediate compounds $PuThF_7$, $PuTh_2F_{11}$, $PuUF_7$, PuU_2F_{11} have been optimized while the data of the LiF, UF_4 and PuF_3 end-members and LiF–ThF_4 and LiF–UF_4 intermediate compounds have been taken from literature [8,9] and in case of ThF_4 from our previous work [6] in which the heat capacity of ThF_4 was revised.

As observed experimentally by Gilpatrick et al. [10], two intermediate compounds ($CeThF_7$, $CeTh_2F_{11}$) are stable in the CeF_3–ThF_4 binary system. Therefore, in absence of any other experimental data the most straightforward assumption was made and compounds with similar stoichiometry were supposed to be present also in the ThF_4–PuF_3 and UF_4–PuF_3 systems. Estimation of their thermodynamic properties ($\Delta_f H^0(298)$, $S^0(298)$, $C_p(T)$) were made based on the weighted average from the properties of their end-members and adding a contribution related to the compounds formation reaction. The enthalpy and entropy change at 298.15 K for these reactions ($MF_4 + PuF_3 = MPuF_7$ and $2MF_4 + PuF_3 = M_2PuF_{11}$ with M = Th, U) were assumed to be identical to the same quantities for the reactions $ThF_4 + CeF_3 = ThCeF_7$ and $2ThF_4 + CeF_3 = Th_2CeF_{11}$. No change in the $C_p(T)$ function was considered.

2.2. Solid solution

The total Gibbs energy of a solution is generally described by three terms: the sum of the standard Gibbs energy of the constituents, an ideal mixing term and an excess term. The latter term is usually unknown and it has been optimized in this work. In case of solid solution, the sublattice model [11] was used considering the cationic species involved (Pu^{3+}, Th^{4+} or U^{4+}) on the first sublattice and the anionic species (F^-) on the second sublattice. Using this model, the equivalent cationic (y_A, y_B,..) and anionic fraction (y_X, y_Y,..) are defined as follows:

$$y_A = q_A n_A/(q_A n_A + q_B n_B + \ldots) \quad (2)$$

$$y_X = q_X n_X/(q_X n_X + q_Y n_Y + \ldots) \quad (3)$$

where n_i are the number of moles of ion i in solution and q_i are the absolute ionic charges. In a binary system with a common anion A,B/F, the equivalent anionic fraction y_{F^-} is equal to one and the excess Gibbs energy is expressed as a polynomial in the equivalent cationic fractions y_A and y_B:

$$\Delta G^{xs} = \sum_{i\geqslant 1}\sum_{j\geqslant 1} y_A^i \cdot y_B^j \cdot L_{i,j} \quad (4)$$

where $L_{i,j}$ is the parameter to be optimized.

In case of both the ThF_4–PuF_3 and UF_4–PuF_3 systems, the formation of a solid solution in the PuF_3-rich corner has been considered based on the experimentally confirmed solid solution in the ThF_4–CeF_3 phase diagram [10]. The same parameters as optimized for the (Ce,Th) F_x solid solution in our previous study [6] were also

Table 1
The $\Delta_f H^0(298.15)$ (kJ mol^{-1}), $S^0(298.15)$ (J K^{-1} mol^{-1}) and C_p (J K^{-1} mol^{-1}) data of pure compounds used in this study.

Compound	$\Delta_f H^0(298.15)$	$S^0(298.15)$	$C_p = a + b\,T + cT^2 + dT^{-2}$			
			a	$b\,T$	$c\,T^2$	$d\,T^{-2}$
LiF (cr)	−616.931	35.66	43.309	$1.6312\cdot10^{-2}$	$5.0470\cdot10^{-7}$	$-5.691\cdot10^{5}$
LiF (l)	−598.654	42.962	64.183	–	–	–
ThF_4 (cr)	−2097.900	142.05	122.173	$8.3700\cdot10^{-3}$	–	$-1.255\cdot10^{6}$
ThF_4 (l)	−2103.654	101.237	170.0	–	–	–
UF_4 (cr)	−1914.200	151.70	114.519	$2.0555\cdot10^{-2}$	–	$-4.131\cdot10^{5}$
UF_4 (l)	−1914.658	115.400	174.74	–	–	–
PuF_3 (cr)	−1586.694	126.11	104.08	$7.070\cdot10^{-4}$	–	$-1.036\cdot10^{6}$
PuF_3 (l)	−1568.813	109.33	130.00	–	–	–
$LiThF_5$ (cr)	−2719.490	181.89	165.482	$2.468\cdot10^{-2}$	$5.047\cdot10^{-7}$	$-1.824\cdot10^{6}$
Li_3ThF_7 (cr)	−3960.259	236.1	282.100	$5.730\cdot10^{-2}$	$1.514\cdot10^{-6}$	$-2.962\cdot10^{6}$
$LiTh_2F_9$ (cr)	−4822.329	324.29	287.655	$3.305\cdot10^{-2}$	$5.047\cdot10^{-7}$	$-3.079\cdot10^{6}$
$LiTh_4F_{17}$ (cr)	−9021.140	609.0	532.001	$4.979\cdot10^{-2}$	$5.047\cdot10^{-7}$	$-5.589\cdot10^{6}$
Li_4UF_8 (cr)	−4347.620	357.55	287.755	$8.5804\cdot10^{-2}$	$2.0188\cdot10^{-6}$	$-2.690\cdot10^{6}$
$Li_7U_6F_{31}$ (cr)	−15826.900	1230.82	990.279	$2.3751\cdot10^{-1}$	$3.5329\cdot10^{-6}$	$-6.463\cdot10^{6}$
LiU_4F_{17} (cr)	−8293.761	644.70	501.387	$9.8532\cdot10^{-2}$	$5.0470\cdot10^{-7}$	$-2.222\cdot10^{6}$
Th_2PuF_{11} (cr)	−5737.637	454.41	348.424	$1.7447\cdot10^{-2}$	–	$-3.546\cdot10^{6}$
U_2PuF_{11} (cr)	−5370.237	473.71	333.117	$4.1817\cdot10^{-2}$	–	$-1.862\cdot10^{6}$

used for the description of the (Pu,Th) F_x and (Pu,U) F_x solid solutions, thus:

$$\Delta G^{xs} = y_{Pu^{3+}} \cdot y^3_{Th^{4+}} \cdot 30,000 \text{ J mol}^{-1} \quad (5)$$

$$\Delta G^{xs} = y_{Pu^{3+}} \cdot y^3_{U^{4+}} \cdot 30,000 \text{ J mol}^{-1} \quad (6)$$

where the y terms are the site fractions of the given species. The ThF_4–UF_4 system forms a continuous solid solution [12,13] as described by the following relation:

$$\Delta G^{xs} = y_{U^{4+}} \cdot y_{Th^{4+}} \cdot 400 \text{ J mol}^{-1}. \quad (7)$$

In addition, the formation of solid solutions within the LiF–ThF_4 intermediate compounds and LiF–UF_4 intermediate compounds is well-established and the data for the Gibbs energy description were taken from our previous work (see Table 2 in [5]).

2.3. Liquid solution

In case of the liquid solution, the description of the excess Gibbs parameter is given by the modified quasi-chemical model proposed by Pelton et al. [14]. This model is suitable for the description of ionic liquids as the composition of maximum short range ordering can be changed by varying the ratio between two parameters: the cation-cation coordination numbers $Z^A_{AB/FF}$ and $Z^B_{AB/FF}$ (in the present case with only one type of anion) which are listed in Table 2. Moreover, the same model has been used in previous works performed at Institute for Transuranium Elements (ITU) thus it allows an extension of the thermodynamic database developed.

The short range ordering is defined by the quadruplet approximation and the model treats also the second-nearest neighbour interactions, cation–cation and anion–anion. Let A and B be two generic cations and F the fluorine anion, the formation of the generic second-nearest neighbour pair (A–F–B) is given by the following reaction:

$$(A-F-A)+(B-F-B) = 2(A-F-B) \quad \Delta g_{AB/F} \quad (8)$$

where $\Delta g_{AB/F}$ is the Gibbs energy change related to the pair formation and it is an empirical parameter of the model, which may be composition dependent. It can be expanded in polynomial form such as:

$$\Delta g_{AB/F} = \Delta g^0_{AB/F} + \sum_{i\geqslant 1} g^{i0}_{AB/F}\chi^i_{AB/F} + \sum_{j\geqslant 1} g^{0j}_{AB/F}\chi^j_{BA/F} \quad (9)$$

where $\Delta g^0_{AB/F}$ and $g^{ij}_{AB/F}$ are composition independent coefficients while the dependence of the parameter on composition is given by the $\chi_{AB/F}$ terms, defined as function of the cation–cation pair fractions X_{AA}, X_{BB}, X_{AB}.

In general, for a molten fluoride salt solution the charge-neutrality condition for the ABFF quadruplets must be fulfilled and it is done by the definition of the cation–cation coordination numbers respecting the absolute cationic and anionic charges (q_A, q_B,..):

$$\frac{q_A}{Z^A_{AB/FF}} + \frac{q_B}{Z^B_{AB/FF}} = \frac{q_F}{Z^F_{AB/FF}} + \frac{q_F}{Z^F_{AB/FF}}. \quad (10)$$

Table 2
Cation–cation coordination numbers of the liquid solution.

A	B	$Z^A_{AB/FF}$	$Z^B_{AB/FF}$
Li^+	Li^+	6	6
Pu^{3+}	Pu^{3+}	6	6
Th^{4+}	Th^{4+}	6	6
U^{4+}	U^{4+}	6	6
Li^+	Pu^{3+}	2	6
Li^+	Th^{4+}	2	6
Li^+	U^{4+}	2	6
Pu^{3+}	Th^{4+}	6	3
Pu^{3+}	U^{4+}	6	3
Th^{4+}	U^{4+}	6	6

Using the same approach adopted for the solid solution, the liquid solution for the ThF_4–PuF_3 and UF_4–PuF_3 systems have been described using the same parameters assessed for the ThF_4–CeF_3 system [6], which are given below:

$$\Delta g_{PuU/FF} = \Delta g_{PuTh/FF} = +335 - 6.28T + 2093\chi_{Pu(U,Th)/F} \quad \text{J mol}^{-1} \quad (11)$$

The excess Gibbs parameters for the remaining binary systems have been taken from our previous works [5,15] and for completeness they are listed below. No excess parameters were considered in case of the ThF_4–UF_4 system. That is, the ThF_4–UF_4 liquid was assumed to be ideal (*i.e.* $\Delta g_{ThU/FF} = 0$).

$$\Delta g_{LiTh/FF} = -10,883 + \chi_{LiTh/F}(-6697 + 2.93T) + \chi_{ThLi/F}(-20930 + 19.25T) \text{ J mol}^{-1} \quad (12)$$

$$\Delta g_{LiU/FF} = -16,115 + \chi_{LiU}(-711.6 - 1.256T) + \chi_{ULi}(-1172 - 8.371T) \text{ J mol}^{-1} \quad (13)$$

$$\Delta g_{LiPu/FF} = -2930 - 3348.6\chi_{LiPu} \text{ J mol}^{-1} \quad (14)$$

Using the data of the binary phase diagrams, all the ternary phase diagrams have been extrapolated using the Kohler or Kohler/Toop interpolation methods depending on the symmetric or asymmetric nature of the system. In fact, the alkali fluoride LiF has a very different chemical behaviour and higher ionic nature compared to the all the other compounds which are actinide fluorides, thus it was considered as asymmetric component. Some ternary parameters ($\Delta g^{ijk}_{AB(C)}$) have to be introduced to optimize the phase diagram according to the experimental data available [16,17] and they are listed below.

$$\Delta g^{001}_{LiTh(Pu)/FF} = -7953 \text{ J mol}^{-1} \quad (15)$$

$$\Delta g^{001}_{LiU(Pu)/FF} = -6698 \text{ J mol}^{-1} \quad (16)$$

$$\Delta g^{001}_{PuTh(Li)/FF} = +20,930 \text{ J mol}^{-1} \quad (17)$$

$$\Delta g^{001}_{PuU(Li)/FF} = +16,744 \text{ J mol}^{-1} \quad (18)$$

Since the optimization was performed separately on the two ternary systems (LiF–ThF_4–PuF_3 and LiF–UF_4–PuF_3), the parameters obtained for the proxy systems Th- and U- containing are different. However, the values have the same order of magnitude in agreement with the assumptions made.

3. Experiment

To confirm the thermodynamic assessment developed, some selected ternary compositions have been prepared and analysed in this study. The samples were synthesized using the CeF_3, LiF and ThF_4 pure components. In fact, it seems to be adequate as first step to carry out most of the experiment using ThF_4 as proxy compound to UF_4 and CeF_3 as proxy compound to PuF_3. Once possible, few measurements with PuF_3 and UF_4 will be necessary to confirm the conclusions made.

The samples analysed in this study were prepared by mixing stoichiometric quantities of the LiF and CeF_3, both obtained from AlfaAesar, and ThF_4 obtained from Rhodia (France). Since all the fluorides salts have tendency to absorb water molecules, LiF and CeF_3 compounds were subjected, prior the mixing, to a drying process at 623 K for 3 h under Argon atmosphere. In case of ThF_4, there

is an additional tendency to oxidize to form oxyfluorides impurities that can dissolve in the salt. These impurities have been converted into fluorides using a fluorinating agent, NH_4HF_2, using the procedure described in our previous work [18]. Afterwards, the purity of the salt was checked for its melting point using DSC. The powder prepared by mixing the pure compounds was filled into a specific crucible [13] designed for the DSC instrument employed in our laboratories (SETARAM MD-HTC96), which serves as barrier for the instrument detector against the corrosive fluoride vapours. It is important to notice that the whole preparation is made inside an Argon glove box to avoid possible deterioration of the samples due to oxygen and water molecules.

The samples were analysed using DSC for the experimental determination of the transition temperatures. The instrument consists of two compartments, resp. the reference and the sample compartment, that are subjected to the same controlled temperature program. For the measurements, a standard program consisting of four heating cycles up to 1573 K has been selected. The heating ramp was performed with constant heating rate of 10 K/min, while the cooling ramp was performed at different cooling rates for each cycle (5 K/min, 7 K/min, 10 K/min and 15 K/min) in order to correct for the supercooling effect, as explained below. The instrument operates under Argon flow to avoid the oxidation of the crucible at high temperature. During the experiments, a series of thermocouples placed around the compartments detects the temperature and the heat flow signal. When the salt undergo a transition, the event is registered by the instrument as a peak, giving information on the phase transitions and their relative temperatures.

In order to validate the developed thermodynamic database, seven selected compositions of the LiF–ThF_4–CeF_3 system were prepared and measured using DSC for the identification of the melting behaviour. The exact compositions and the measured temperatures are listed in Table 3, where T_{meas} is the average value of the four consecutive heating cycles and where the maximum deviation observed was not larger than ±10 K. For all the measured compositions, three phase transitions between the room temperature and 1523 K were identified, which is in agreement with the calculation. They represent respectively the ternary eutectic (Equilib. A), the solid solution stability limit (Equilib. B) and the liquidus point (Equilib. C). While in case of the first two transitions (A and B) the temperatures were identified as the onset points of the peaks during the heating process, the liquidus transition (C) was sometimes difficult to identify as it tends to form a broad shoulder in the heat flow signal. A more precise determination can be obtained from the cooling curves, which show a much sharper peak. However, during the cooling process the temperatures were not deduced directly as the onset temperatures of the peak due to supercooling event. The liquidus temperature was obtained by extrapolation to zero cooling rate by a straight line using the points measured at different rates.

The LiF–ThF_4–CeF_3 samples were prepared focusing on a very narrow range of compositions which is believed to be the most important for the MSFR fuel. The concentration ratio of LiF/ThF_4 has been set to a value suggested by preliminary version of the ternary phase diagram and close to the minimum temperature in the LiF–ThF_4 pseudo binary phase diagram ($X_{PuF_3} \sim 3\%$). The salt mixtures were then prepared by varying only the concentration of CeF_3 (proxy to PuF_3) in the mixture in order to investigate the influence of trifluoride salts concentration on the liquidus point and identify the composition of the minimum value. The lowest liquidus point was measured at 867.0 K for the LiF–ThF_4–CeF_3 (77.7–19.0–3.3) composition as reported in Table 3.

Table 3
Phase equilibria in the LiF–ThF_4–CeF_3 system measured for the selected ternary compositions and the calculated transition temperatures for LiF–ThF_4–PuF_3 system (values in italic).

Composition			Equilibrium A		Equilibrium B		Equilibrium C	
x_{LiF}	x_{ThF_4}	x_{CeF_3/PuF_3}	T_{meas}	T_{calc}	T_{meas}	T_{calc}	T_{meas}	T_{calc}
0.789	0.192	0.019	818	*820*	828	*823*	885	*874*
0.778	0.190	0.032	825	*820*	832	831	*889*	*859*
0.777	0.190	0.033	824	*820*	830	*832*	867	*857*
0.777	0.189	0.034	819	*820*	831	*833*	872	*856*
0.776	0.189	0.035	822	*820*	831	*835*	870	*855*
0.775	0.189	0.036	824	*820*	833	*837*	884	*854*
0.767	0.186	0.047	821	*820*	829	*848*	874	*876*

4. Results

4.1. Binary systems ThF_4–PuF_3 and UF_4–PuF_3

Based on the thermodynamic data described in the Section 2, the ThF_4–PuF_3 and UF_4–PuF_3 phase diagrams have been calculated and they are shown in Figs. 1 and 2, respectively. As discussed above, no experimental data have been found in literature for these two systems and thus no direct optimization was possible. Therefore, the optimization of the unknown parameters was done based on the proxy system ThF_4–CeF_3 [6,10]. The main difference observed between the ThF_4–CeF_3 phase diagram and the assessed ThF_4–PuF_3 and UF_4–PuF_3 phase diagrams is the absence in the latter two systems of the intermediate compounds $PuThF_7$ and $PuUF_7$, which are calculated to be unstable with their thermodynamic properties estimated from the one of $CeThF_7$ and $CeUF_7$. In order to reduce this discrepancy, one of the possibilities would be to force the stability of the compounds by varying their thermodynamic properties. However, since there is no experimental evidence for the compounds stability and no indications on their decomposition temperatures, it is not obvious how to optimize the thermodynamic properties and further optimization was not undertaken.

Although there are some differences on the phase fields in the solid state, all the three phase diagrams ThF_4–CeF_3, ThF_4–PuF_3 and UF_4–PuF_3 show a very similar trend of the liquidus line. We must note here that the description of the liquidus lines are of major concern for the safety of the molten salt fuel as they determine the stability limit of the liquid phase at which the molten salt mixture must be maintained. The comparison between the liquidus line of the three systems and the experimental data for ThF_4–CeF_3 system is shown in Fig. 3. Realising the fact that ThF_4 and UF_4 have slightly different melting points, which explains the discrepancy in the right side of the phase diagram, all the data are in very good agreement.

4.2. Ternary systems LiF–ThF_4–PuF_3 and LiF–UF_4–PuF_3

Two ternary systems have been assessed in this work for the first time: LiF–ThF_4–PuF_3 and LiF–UF_4–PuF_3. Based on the thermodynamic description of all the sub-binary systems, the ternary phase diagrams have been extrapolated using the Kohler/Toop formalism and assuming LiF as asymmetric compound. No evidences have been found in literature on the existence of ternary compounds, hence none were considered in this study. However, some ternary excess Gibbs parameters have to be considered in order to reproduce at best the two sets of experimental data, measured by Barton et al. [16] and Ignatiev et al. [17]. The first work describes the solubility of CeF_3 in four LiF–ThF_4 compositions (T = 873 K and T = 1073 K) while Ignatiev et al. have measured

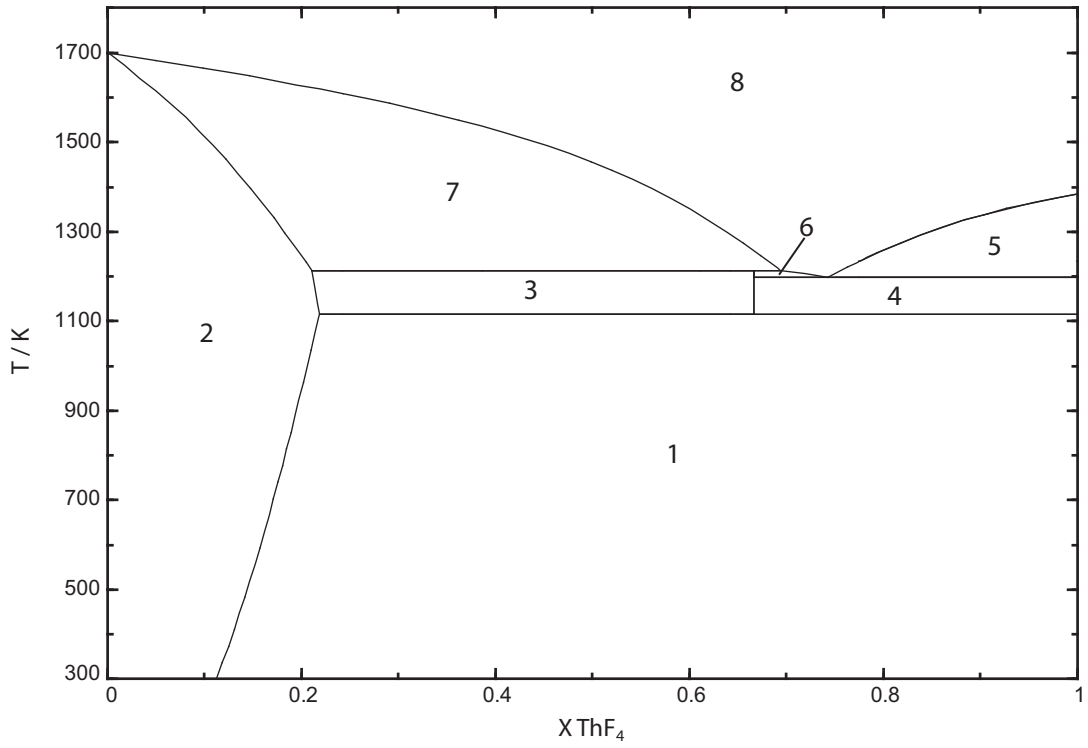

Fig. 1. The ThF_4–PuF_3 calculated phase diagram assessed in this study. Phase fields: (1) $(Pu_{1-x}Th_x)F_{3+x}$ (ss) + ThF_4 (2) $(Pu_{1-x}Th_x)F_{3+x}$ (ss) (3) $(Pu_{1-x}Th_x)F_{3+x}$ (ss) + $PuTh_2F_{11}$ (4) $PuTh_2F_{11}$ + ThF_4 (5) ThF_4 + liq. (6) $PuTh_2F_{11}$ + liq. (7) $(Pu_{1-x}Th_x)F_{3+x}$ (ss) + liq. (8) Liquid.

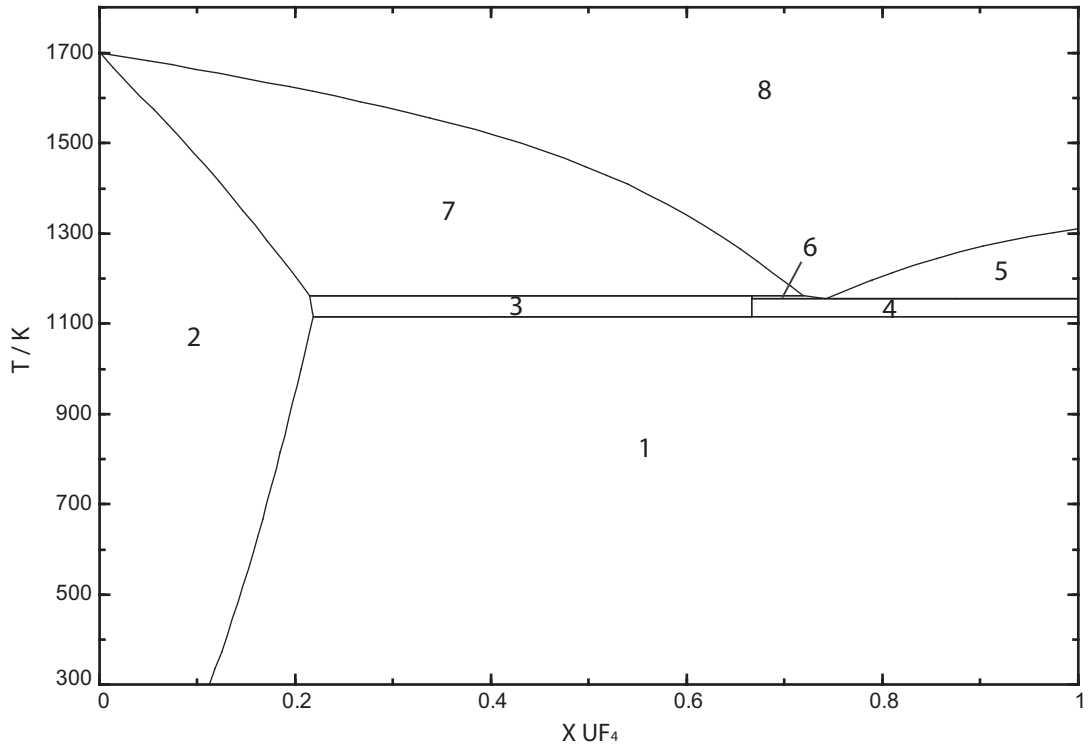

Fig. 2. The UF_4–PuF_3 calculated phase diagram assessed in this study. Phase fields: (1) $(Pu_{1-x}U_x)F_{3+x}$ (ss) + UF_4 (2) $(Pu_{1-x}U_x)F_{3+x}$ (ss) (3) $(Pu_{1-x}U_x)F_{3+x}$ (ss) + PuU_2F_{11} (4) PuU_2F_{11} + UF_4 (5) UF_4 + liq. (6) PuU_2F_{11} + liq. (7) $(Pu_{1-x}U_x)F_{3+x}$ (ss) + liq. (8) Liquid.

the solubility of PuF_3 in two LiF–ThF_4 solvent compositions as function of temperature. The agreement obtained between the experimental data and the calculations is shown in Figs. 4 and 5 respectively, where the solubility of PuF_3 in LiF–ThF_4 solvent is represented by a solid line and the solubility of PuF_3 in LiF–UF_4 solvent is represented by a dashed line.

The liquidus projections of the LiF–ThF_4–PuF_3 and LiF–UF_4–PuF_3 ternary phase diagrams are shown in Figs. 6 and 7 respectively,

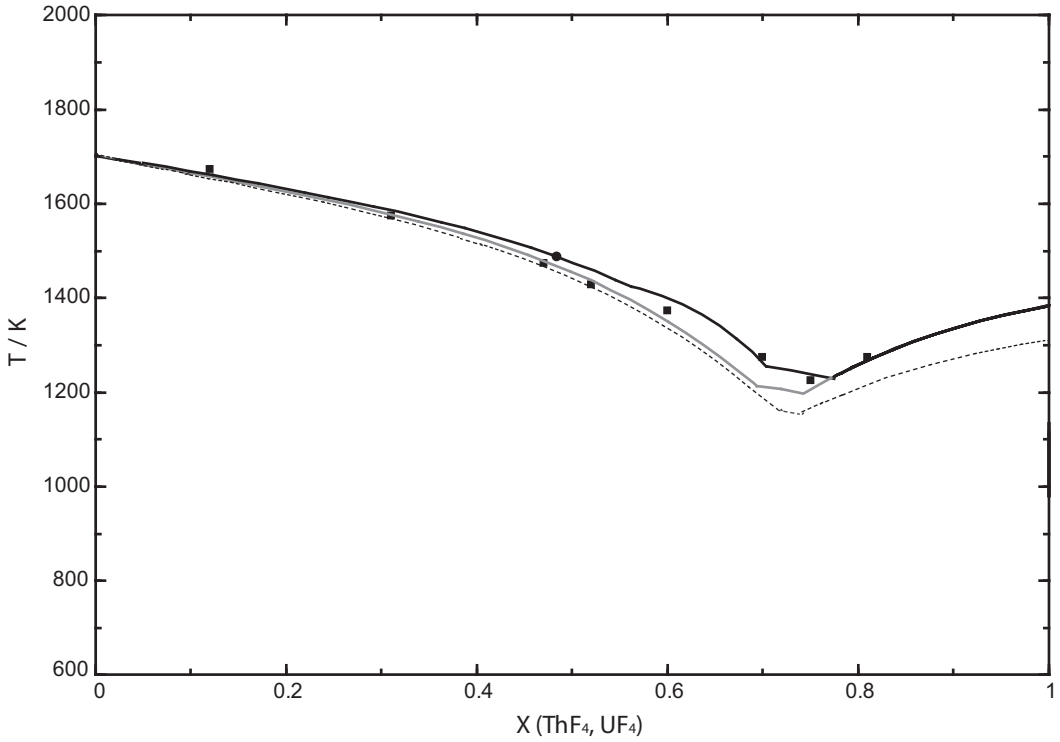

Fig. 3. Comparison between the calculated liquidus lines for the ThF_4–CeF_3 system (black solid line), ThF_4–PuF_3 system (grey solid line) and UF_4–PuF_3 system (dashed line). (■) Data by Gilpatrick et al. [10] and (•) Data by Beneš et al. [6], both for ThF_4–CeF_3 system.

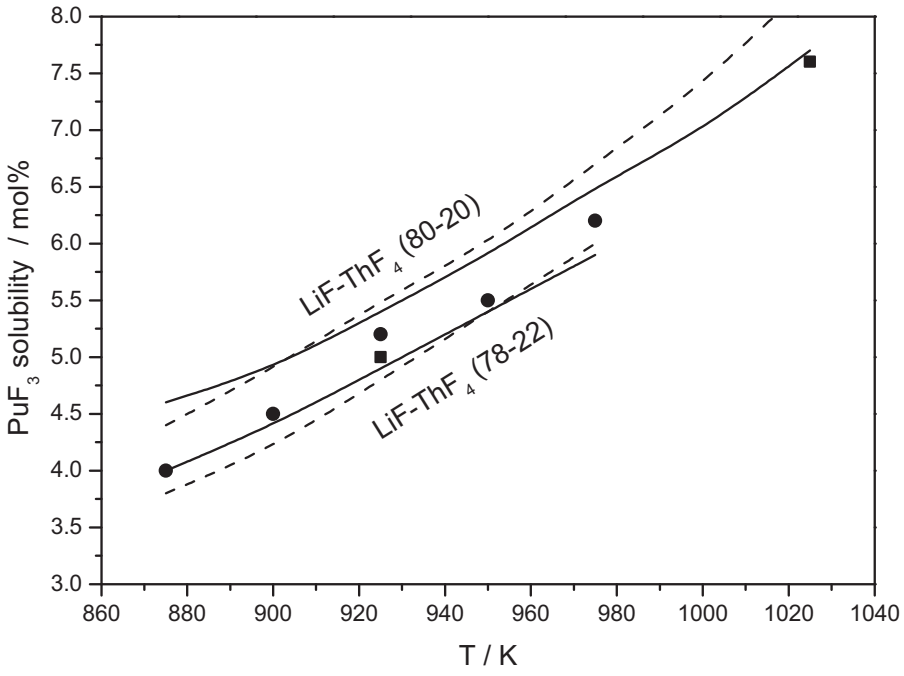

Fig. 4. Calculated solubility of PuF_3 in LiF–ThF_4 mixtures (solid line) and LiF–UF_4 mixtures (dashed line) as a function of temperature. (■) and (•) Experimental data on PuF_3 solubility in LiF–ThF_4 (80–20) solvent and LiF–ThF_4 (78–22) solvent, respectively [17].

showing a very similar shape. In case of the LiF–ThF_4–PuF_3 system, seven invariant points have been found (Table 4) while in case of LiF–UF_4–PuF_3 five invariants points were identified (Table 5).

To validate the database developed, the experimental results have been compared with the calculated equilibrium temperature and a good agreement has been found (Table 3), showing a higher liquidus temperatures in the experiments. In Fig. 8, the experimental points obtained for five compositions (X_{CeF_3} = 3.2, 3.3, 3.4, 3.5 and 3.6 mol%) have been compared with the calculated pseudo-binary LiF–ThF_4 phase diagram having fixed composition of PuF_3. Considering the temperature range of the whole binary phase diagram the comparison between the calculation and the experiment

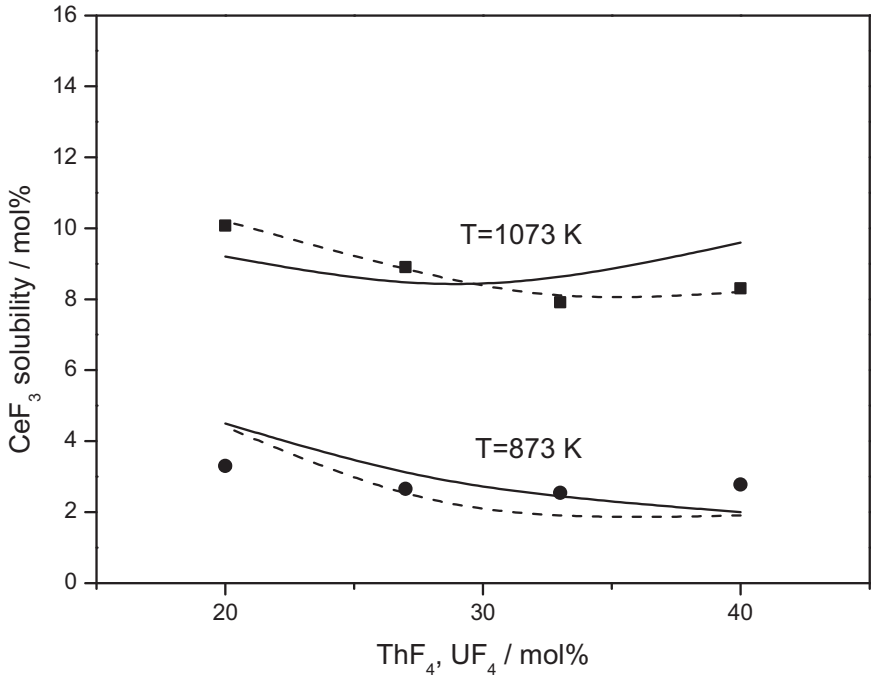

Fig. 5. Calculated solubility of PuF_3 in the LiF–ThF_4 solvent (solid line) and in the LiF–UF_4 solvent (dashed line) as function of ThF_4/UF_4 composition for $T = 873$ K and $T = 1073$ K (■) and (•) Experimental data on CeF_3 solubility in different LiF–ThF_4 mixtures at $T = 1073$ K and $T = 873$ K, respectively [16].

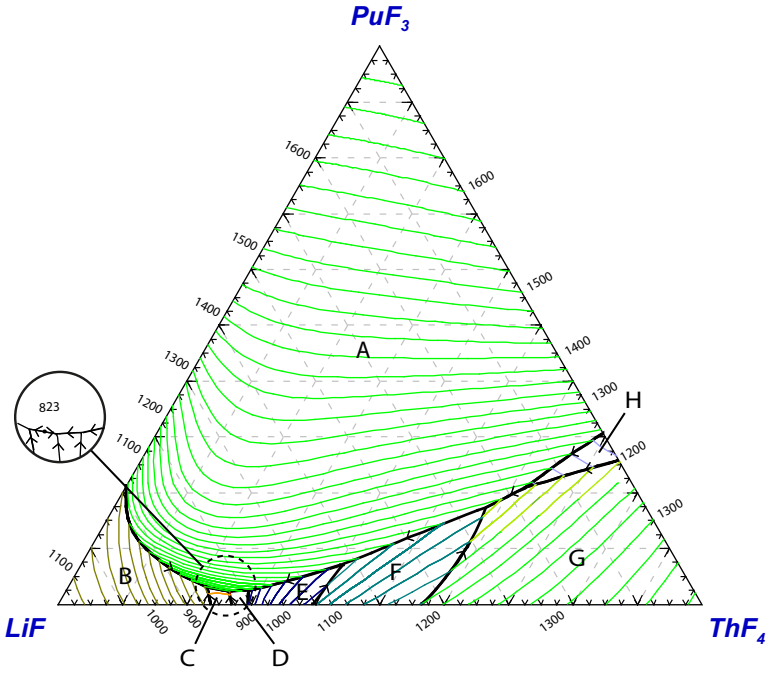

Fig. 6. The liquidus projection of the LiF–ThF_4–PuF_3 system assessed in this study. Primary crystallization phase fields: (A) (Pu,Th) F_x (ss); (B) LiF; (C) Li_3ThF_7; (D) $LiThF_5$; (E) $LiTh_2F_9$; (F) $LiTh_4F_{17}$; (G) ThF_4; (H) $PuTh_2F_{11}$.

reveals fairly good agreement for all measured compositions. In some cases the temperature shifts between the calculation and the experiment for the Equilibrium C are larger than the instrument uncertainty. This may be related to the composition uncertainty ($u(x) = \pm 0.001$) that has larger impact on steep transition lines and to the determination of the peak onset/offset in the DSC signal (for the liquidus transition only the cooling curve can be used). The model represents the best compromise of all the experimental data measured (Equilibrium A, B and C) and available in literature (solubility data on CeF_3 and PuF_3).

5. Fuel optimization

The main result of the thermodynamic modeling described in this work is the complete description of the LiF–ThF_4–PuF_3–UF_4 system. That implies that the thermodynamic properties of each composition can be calculated from the model. Moreover, it also means that an optimization process may be performed by setting the proper criteria in order to find the most suitable composition, as described in this section. In case of the MSFR fuel, one of the main criteria considered is the melting temperature of the salt. A

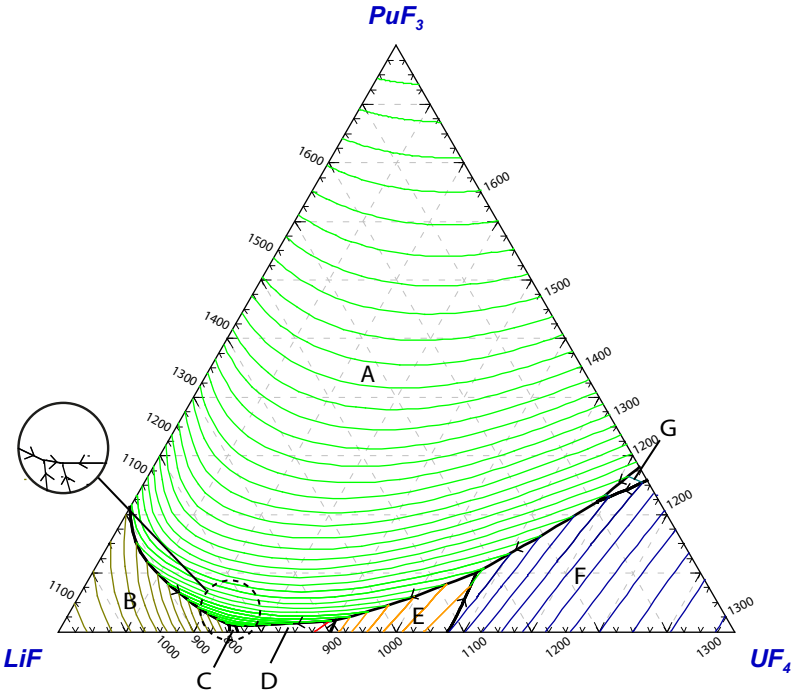

Fig. 7. The liquidus projection of the LiF–UF_4–PuF_3 system assessed in this study. Primary crystallization phase fields: (A) (Pu,U) F_x (ss); (B) LiF; (C) Li_4UF_8; (D) $Li_7U_6F_{31}$; (E) LiU_4F_{17}; (F) UF_4; (G) PuU_2F_{11}.

Table 4
Invariant equilibria and saddle points found in the LiF–ThF_4–PuF_3 system.

x_{LiF}	x_{ThF_4}	x_{PuF_3}	T/K	Type of equilibria	Crystal phases in equilibrium
0.170	0.621	0.209	1115	Quasi-Peritectic	ThF_4, (Th,Pu) F_x (s.s.), $PuTh_2F_{11}$
0.249	0.577	0.174	1089	Quasi-Peritectic	ThF_4, (Th,Pu) F_x (s.s.), $LiTh_4F_{17}$
0.522	0.407	0.071	1011	Quasi-Peritectic	(Th,Pu) F_x (s.s.), $LiTh_4F_{17}$, $LiTh_2F_9$
0.692	0.283	0.025	863	Quasi-Peritectic	(Th,Pu) F_x (s.s.), $LiTh_2F_9$, $LiThF_5$
0.724	0.253	0.023	822	Eutectic	(Th,Pu) F_x (s.s.), $LiThF_5$, Li_3ThF_7
0.731	0.244	0.025	822	Saddle-point	(Th,Pu) F_x (s.s.), Li_3ThF_7
0.753	0.216	0.031	820	Eutectic	(Th,Pu) F_x (s.s.), Li_3ThF_7, LiF

Table 5
Invariant equilibria found in the LiF–UF_4–PuF_3 system.

x_{LiF}	x_{UF_4}	x_{PuF_3}	T/K	Type of equilibria	Crystal phases in equilibrium
0.092	0.686	0.221	1115	Quasi-Peritectic	UF_4, (U,Pu) F_x (s.s.), PuU_2F_{11}
0.332	0.568	0.101	1018	Quasi-Peritectic	UF_4, (U,Pu) F_x (s.s.), LiU_4F_{17}
0.580	0.400	0.019	877	Quasi-Peritectic	(U,Pu) F_x (s.s.), LiU_4F_{17}, $Li_7U_6F_{31}$
0.741	0.246	0.013	765	Quasi-Peritectic	(U,Pu) F_x (s.s.), $Li_7U_6F_{17}$, Li_4UF_8
0.733	0.257	0.010	757	Eutectic	(U,Pu) F_x (s.s.), Li_4UF_8, LiF

low melting point decreases the risk of salt freezing and reduces the problems related with the corrosion of structural materials because it allows lowering operating temperature of the reactor.

As mentioned in the introduction, reactors operating with the $^{232}Th/^{233}U$ cycle have to be started with an initial load of fissile material. An interesting solution is the use of plutonium and minor actinides separated from LWR fuel as initial fissile material achieving at the same time the closure of the fuel cycle. One of the factors that determines the total amount of material that can be added to the salt is the solubility of actinide trifluorides (PuF_3, NpF_3, AmF_3, CmF_3) in the LiF–ThF_4 mixture. Considering this limitation, the initial composition considered for the MSFR fuel contains 5 mol% of PuF_3 which is dissolved in the eutectic composition ^{7}LiF–ThF_4 (78–22 mol%). In order to avoid fluoride corrosion, it is necessary to control the redox potential by setting the right UF_4/UF_3 ratio. It implies that both UF_4 and UF_3 have to be present in the salt and as demonstrated in the MSRE project [19], the ratio UF_4/UF_3 should be around 100 to inhibit the corrosion. In this work, we consider a concentration of 1% UF_4 as the minimum concentration required for redox control and we neglect the contribute of UF_3, as the concentration is so small that will not strongly influence the melting point of the mixture. It is important to notice that the concentration of 1% UF_4 is the minimum required but it may be larger if necessary. Adding to the previous defined salt mixture 1 mol% of UF_4, the initial composition becomes LiF–ThF_4–PuF_3–UF_4 (73.3–20.7–5.0–1.0), which has a calculated melting point equal to 944 K. Fig. 9 shows the LiF–ThF_4 pseudo-binary phase diagram with fixed concentration of PuF_3 and UF_4 equal to 5 mol% and 1 mol%, respectively. As shown, the initial MSFR composition (solid vertical line) does not correspond to the minimum liquidus temperature on the phase diagram and can be further lowered by decreasing the amount of ThF_4. The lowest liquidus temperature is now found at 867 K for the composition LiF–ThF_4–PuF_3–UF_4 (78.0–16.0–5.0–1.0), represented in Fig. 9 by the dashed vertical line. This salt mixture represents a promising candidate for the MSFR fuel according to its physico-chemical properties, but it is necessary to establish whether it also fullfills the reactor physics criteria.

A second fuel option may be based on a lower concentration of PuF_3, which would be compensated with a corresponding amount of $^{235}UF_4$. In fact, the total concentration of fissile material should be kept to the minimum value of 5 mol%. This fuel option, which

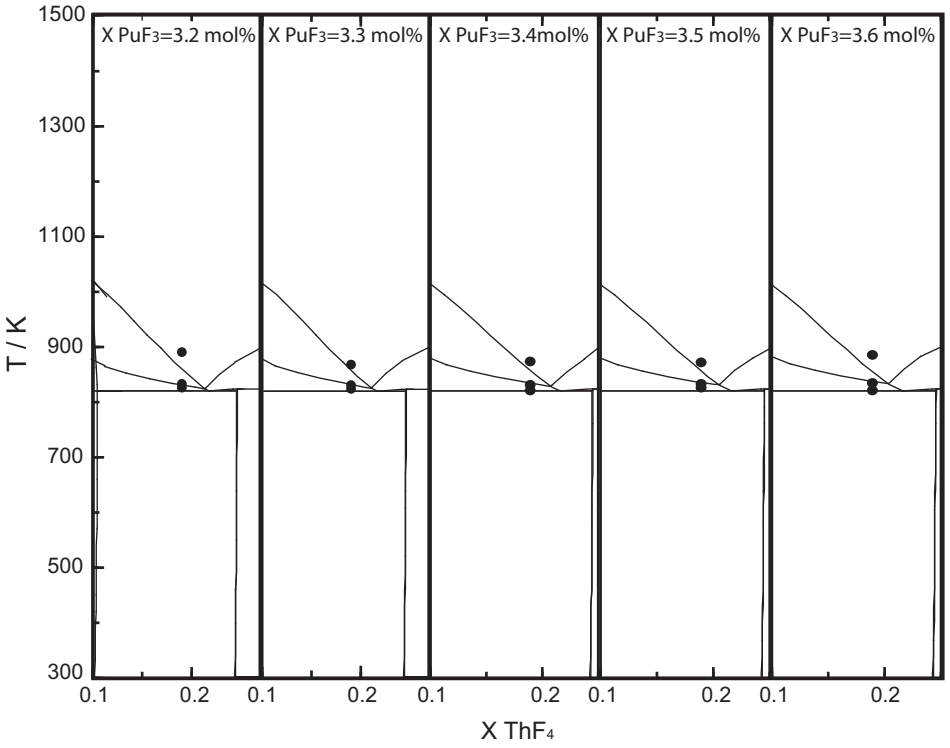

Fig. 8. Comparison between the experimental points measured for five different LiF–ThF_4–CeF_3 compositions and the calculated pseudo binary LiF–ThF_4 phase diagram with fixed amount of PuF_3.

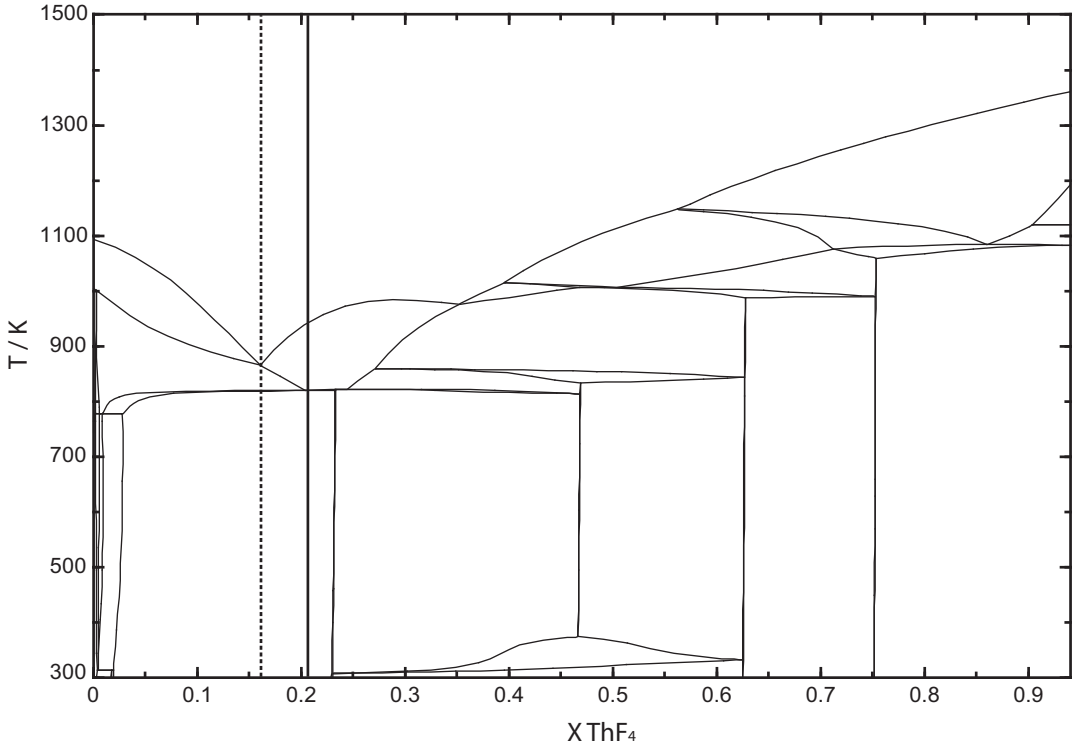

Fig. 9. The pseudo binary LiF–ThF_4 phase diagram having a fixed concentration of 5 mol% PuF_3 and 1 mol% of UF_4. The solid line represent the first considered fuel composition while the dashed line represent the composition showing the lowest liquidus temperature.

does not maximize the waste reduction, has the advantage of offering a lower melting temperature which is significantly influenced by the total amount of PuF_3. From the calculated pseudo-ternary LiF–ThF_4–PuF_3 phase diagram with a fixed composition of 1 mol% UF_4 (Fig. 10), the lowest eutectic is identified for the LiF–ThF_4–PuF_3–UF_4 (75.4–20.6–3.0–1.0) composition at $T = 819$ K. The low melting point of this salt mixture, around 46 K lower than the previous one, makes this composition suitable as candidate fuel

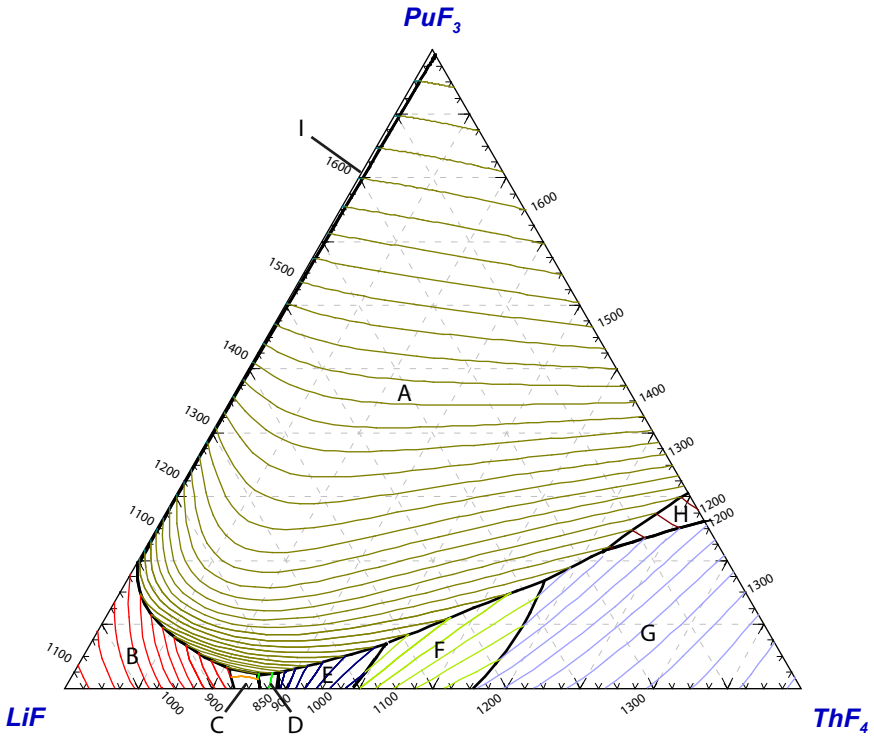

Fig. 10. The calculated LiF–ThF_4–PuF_3 phase diagram with a fixed concentration of UF_4 set to 1 mol%. Primary phase fields: (A) (Pu,Th) F_x (s.ss); (B) LiF; (C) $Li_3(Th, U)F_7$; (D) $Li_7(Th, U)_6F_{31}$; (E) $Li(Th,U)_2F_9$ (F) $Li(Th, U)_4F_{17}$; (G) (Th,U) F_x (s.s.) (H) $PuTh_2F_{11}$ (I) (Pu,U) F_x (s.s.).

Table 6
Influence of the partial substitution of ThF_4 with UF_4 on the most important fuel properties.

Composition	*T* liquidus (K)	*T* boiling (K)	*P* at T_{oper}[a] (Pa)
LiF–ThF_4–UF_4–PuF_3 (75.4–20.6–1.0–3.0)	819	2033	$7.39 \cdot 10^{-4}$
LiF–UF_4–PuF_3 (75.4–21.6–3.0)	842	2002	$1.70 \cdot 10^{-3}$

[a] T_{oper} is the operation temperature defined here as 50 K higher than the liquidus temperature.

Table 7
The potential fuel composition and the related fuel properties.

Composition	*T* liquidus (K)	*T* boiling (K)	*P* at T_{oper}[a](Pa)
LiF–ThF_4–UF_4–PuF_3[b] (73.3–20.7–1.0–5.0)	944 K	2035 K	$4.62 \cdot 10^{-2}$
LiF–ThF_4–UF_4–PuF_3 (78.0–16.0–1.0–5.0)	867 K	2035 K	$5.33 \cdot 10^{-3}$
LiF–ThF_4–UF_4–PuF_3 (75.3–20.6–1.0–3.1)	819 K	2032 K	$7.26 \cdot 10^{-4}$

[a] T_{oper} is the operation temperature defined here as 50 K higher than the liquidus temperature.
[b] Starting fuel composition defined by MSFR concept.

for the MSFR but the proportion of thorium/uranium in the initial fissile load should be optimized based on neutronic calculations and non-proliferation issues.

In fact, keeping the sum of ThF_4 and UF_4 constant while increasing the UF_4/ThF_4 ratio it is possible to increase the fissile concentration in the salt and maintaining the uranium enrichment to reasonable values (<20%) [20]. In order to evaluate the influence of the partial substitution of ThF_4 by UF_4 on the liquidus temperature, we have performed several calculations starting from the LiF–ThF_4–PuF_3–UF_4 (75.4–20.6–3.0–1.0) composition (calculated lowest liquidus point). Considering the extreme case when the total amount of ($ThF_4 + UF_4$) is fully represented by UF_4 the composition becomes LiF–UF_4–PuF_3 (75.4–21.6–3.0) with calculated liquidus temperature of 842 K. Although this value is slightly higher compared to the minimum temperature predicted in case of only 1 mol% of UF_4 present in the mixture, a total increase of 20 K for the extreme case is considered to be acceptable. Moreover, other important properties as vapour pressure and boiling point have been calculated for the two extreme cases and are shown in Table 6. The vapour pressure data have been calculated for the temperature T_{oper}, which is 50 K higher than the liquidus temperature to give enough margin to be considered as a safe operation temperature of the MSFR. The main contribution to the vapour pressure is given by the following gaseous species: LiF, Li_2F_2, Li_3F_3, ThF_4, UF_4 and PuF_3. From the results, it is possible to conclude that the partial substitution of ThF_4 with UF_4 influences the physico-chemical properties of the mixture. However, considering the total amount of ThF_4 and UF_4 constant and increasing the amount of UF_4, it is possible to decrease the uranium enrichment to reasonable values keeping good physico-chemical properties.

6. Conclusions

In this work, the full thermodynamic description of the LiF–ThF_4–PuF_3–UF_4 system has been performed. The binary and ternary systems containing PuF_3 have been assessed for the first time based on the similarities between the proxy compounds (PuF_3/CeF_3 and ThF_4/UF_4) and the experimental data available in literature. The model developed was able to reproduce very well the solubility measurements of CeF_3 and PuF_3 in LiF–ThF_4, giving justification for the assumptions made.

In order to verify the validity of the model developed, the DSC technique has been used to analyse selected LiF–ThF_4–CeF_3 compositions and the results have confirmed the phase

equilibrium predicted. Moreover, using the thermodynamic database developed some potential compositions for the MSFR fuel have been selected based on their physico-chemical properties (mainly based on the melting point). All the considered compositions are summarized in Table 7 and the most important properties for these salt mixtures have been calculated.

All the proposed compositions have a concentration of 1 mol% UF_4, which is the assumed minimum required for redox control via UF_4/UF_3 ratio. However, as explained in this work the concentration of UF_4 required may be larger for neutronic reasons. Therefore the influence of partial substitution of ThF_4 with UF_4 on the different important fuel properties have been investigated and it was concluded to be small for the considered composition.

Acknowledgements

This work was supported by the EVOL project in the 7th Framework Programme of the European Commission (Grant Agreement No. 249696). The authors would like to thank E. Merle-Lucottte and M. Allibert of the Research Group of CNRS Grenoble for the fruitful discussion.

References

[1] S. Delpech, E. Merle-Lucotte, D. Heuer, M. Allibert, V. Ghetta, C. Le-Brun, X. Doligez, G. Picard, J. Fluor. Chem. 130 (2009) 11–17.
[2] W.R. Grimes, N.V. Smith, G.M. Watson, J. Phys. Chem. 62 (1958) 862–866.
[3] R. Thoma, Tech. Rep. ORNL-TM-2256, 1968.
[4] E. Merle-Lucotte, D. Heuer, C. LeBrun, L. Mathieu, R. Brissot, E. Liatard, O. Meplan, A. Nuttin, Fast Thorium Molten Salt Reactors started with Plutonium, in: Proceedings of the International Congress on Advances in Nuclear Power Plants (ICAPP), Reno, USA, 2006.
[5] E. Capelli, O. Beneš, R.J.M. Konings, J. Nucl. Mater. 449 (2014) 111–121.
[6] O. Beneš, R.J.M. Konings, J. Nucl. Mater. 435 (2013) 164.
[7] C.W. Bale, E. Bélisle, P. Chartrand, S.A. Decterov, G. Eriksson, K. Hack, I.H. Jung, Y.B. Kang, J. Melançon, A.D. Pelton, C. Robelin, S. Petersen, CALPHAD 33 (2009) 295–311.
[8] M.W. Chase Jr. (Ed.), NIST-JANAF Thermochemical Tables Fourth Edition, J. Phys. Chem. Ref. Data, Monograph 9 (1998).
[9] R.J.M. Konings, L.R. Morss, J. Fuger, The Chemistry of the Actinide and Transactinide Elements, vol. 4, Springer, Dordrecht, The Netherlands, 2006. chap. 19.
[10] L.O. Gilpatrick, C.J. Barton, H. Insley, Tech. Rep. ORNL-TM-4622, 1970.
[11] A.D. Pelton, CALPHAD 12 (1988) 127–142.
[12] C.F. Weaver, R.E. Thoma, H. Insley, H.A. Friedman, J. Am. Ceram. Soc. 43 (1960) 213.
[13] O. Beneš, M. Beilmann, R.J.M. Konings, J. Nucl. Mater. 405 (2010) 186–198.
[14] A.D. Pelton, P. Chartrand, G. Eriksson, Metall. Trans. 32A (2001) 1409–1416.
[15] O. Beneš, R.J.M. Konings, J. Nucl. Mater. 377 (3) (2008) 449–457.
[16] C.J. Barton, L.O. Gilpatrick, J.A. Bornmann, H.H. Stone, T.N. McVay, H. Insley, J. Inorg. Nucl. Chem. 33 (1970) 337–344.
[17] V. Ignatiev, O. Feynberg, A. Merzlyakov, A. Surenko, A. Zagnitko, V. Subbotin, R. Fazilov, M. Gordeev, A. Panov, A. Toropov, in: Proceedings of ICAPP-2012, Chicago, USA, 2012.
[18] E. Capelli, O. Beneš, M. Beilmann, R.J.M. Konings, J. Chem. Thermodyn. 58 (2013) 110–116.
[19] E.L. Compere, S.S. Kirslis, E.G. Bohlmann, F.F. Blankenship, W.R. Grimes, Tech. Rep. ORNL-4865, 1975.
[20] D. Heuer, E. Merle-Lucotte, M. Allibert, M. Brovchenko, V. Ghetta, P. Rubiolo, Ann. Nucl. Energy 64 (2014) 421–429.